

Angiboust, S., Cambeses, A., Hyppolito, T., Glodny, J., Monié, P., Calderón, M., and Juliani, C., 2018, A 100 Ma-long window onto mass flow processes in the Patagonian Mesozoic subduction zone (Diego de Almagro Island, Chile): GSA Bulletin, <https://doi.org/10.1130/B31891.1>.

Data Repository

Electronic Appendix DR1. petrology and P-T estimates for amphibolitization conditions in the SASZ

Electronic Appendix DR2. Location of ^{39}Ar - ^{40}Ar ablation sites for the five samples studied.

Electronic Appendix DR3. Cawood cumulative zircon ages plots

Table DR1. Full Rb-Sr dataset

Table DR2. Full ^{39}Ar - ^{40}Ar dataset

Table DR3. Full U-Pb dataset; U-Th-Pb SHRIMP data for for samples: #48c; #47a; #39; and #43. d (%) = $100 \times (1 - 206/238 \text{ age} / 207/235 \text{ age})$; f^{206} % = $(\text{common } ^{206}\text{Pb} / \text{total } ^{206}\text{Pb}) \times 100$.

All uncertainties are at 95%.

Table DR4. GPS coordinates of sampling localities

Electronic Appendix 1: Petrology of the Seno Arcabuz Shear Zone (SASZ)

Electron probe analyses

Electron probe micro-analyses have been characterized at the GFZ Potsdam with a JEOL-JXA 8230 probe under common analytical conditions (15 kV, 20 nA, wavelength-dispersive spectroscopy mode), using a 10 μm beam. The standards used for the calibration are the following: orthoclase (Al, Si, K), fluorite (F), rutile (Ti), Cr_2O_3 (Cr), wollastonite (Ca), tugtupite (Cl), albite (Na), MgO (Mg), Fe_2O_3 (Fe) and rhodonite (Mn). Amphibole compositions were normalized following the scheme of Leake et al. (1997) with Fe^{3+} estimated using the average normalization-factor. Chlorite and white mica were normalized to 28 and 11 oxygens, respectively, assuming $\text{Fe}_{\text{total}}=\text{Fe}^{2+}$. Plagioclase and epidote were normalized to 8 and 12.5 oxygens, respectively, assuming Fe_{total} as Fe^{3+} . Mineral abbreviations used are after Whitney and Evans (2010).

Petrography and mineral chemistry

Mafic rocks from the SASZ are generally formed by foliation-parallel hornblende crystals tightly interbedded with epidote or plagioclase richer layers (Fig.S1a). Quartz richer bands are also present. Minor amounts of biotite dispersed in the matrix and systematically parallel to the foliation are visible. Amphiboles sometimes exhibit tremolitic cores, hornblende mantles and thin tremolite overgrowths (**Figs.S1 and S2a,b,c**). Flattened plagioclase porphyroclasts are always present, exhibiting myrmekitic textures. Anorthite-richer cores (An_{25-30}) are rimmed by an albite rich plagioclase (An_{2-5}). In one sample a 5mm-thick leucocratic band parallelized to the main amphibolite foliation, comprising quartz and myrmekitic plagioclase recalls the texture of some trondhjemitic segregates observed in the adjacent Lazaro unit (Angiboust et al., 2017).

Metasediments are characterized by large amounts of quartz (>40 vol.%) and foliation parallel mica-rich layers wrapping plagioclase, garnet or staurolite porphyroclasts (**Fig.S1c,d**). Garnet exhibits Mn and Ca richer cores and shows an increase in Mg towards the rims and along garnet healed fractures (**Fig.S2d**). The plagioclase is myrmekitic, with anorthite rich cores (An_{24-30}) and albite rich rims (An_{1-2}). The relationships between biotite and muscovite suggest that larger amounts of biotite were present at peak conditions and a large part of them have been replaced by muscovite along shear bands during post-peak deformation (**Fig.S3a,b**). Very thin (10 μm -sized) celadonite-rich (phengitic) rims with silica contents comprised between 3.3 and 3.4 pfu are very commonly observed around muscovite crystals aligned along the main foliation (**Fig.S1f**). Importantly, these rims form randomly

around muscovite crystals and do not show peculiar orientation (“static overgrowth”).

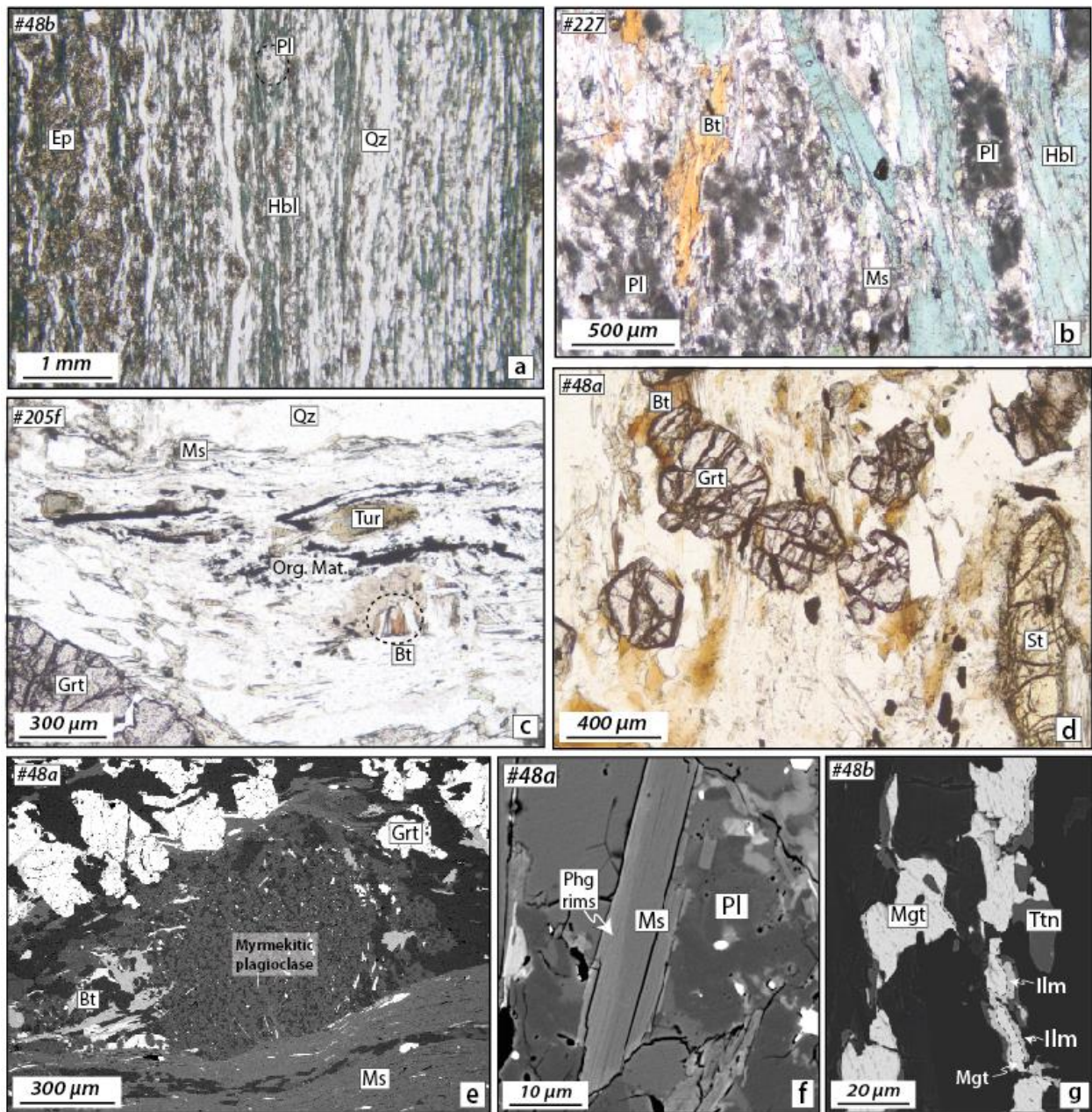


Fig.S1.a : Representative optical microscope view (natural light) of a qtz-bearing tuff from the SASZ with alternance of Qtz-Ab rich layers and Ep-Hbl rich layers. Note the very fine grain size and the pervasive mineral orientation due to mylonitization. b. Amphibolite from the SASZ showing biotite, plagioclase and hornblende in textural equilibrium. c. Metasediment from the SASZ showing the relationship between biotite, muscovite, garnet, tourmaline (Tur) and the main foliation (natural light). Org.Mat.: organic matter. d. Microtextural relationship between garnet, biotite and staurolite in a metapelite from the SASZ. e. SEM back scattered image showing a myrmekitic plagioclase wrapped in the foliation of a garnet micaschist. Note the pressure shadows filled by biotite. f. SEM BSE microphotograph showing a muscovite grain rimmed by a phengite-rich composition. g. SEM BSE

image showing magnetite grains replaced by ilmenite (amphibolitization) further replaced by titanite (greenschist facies).

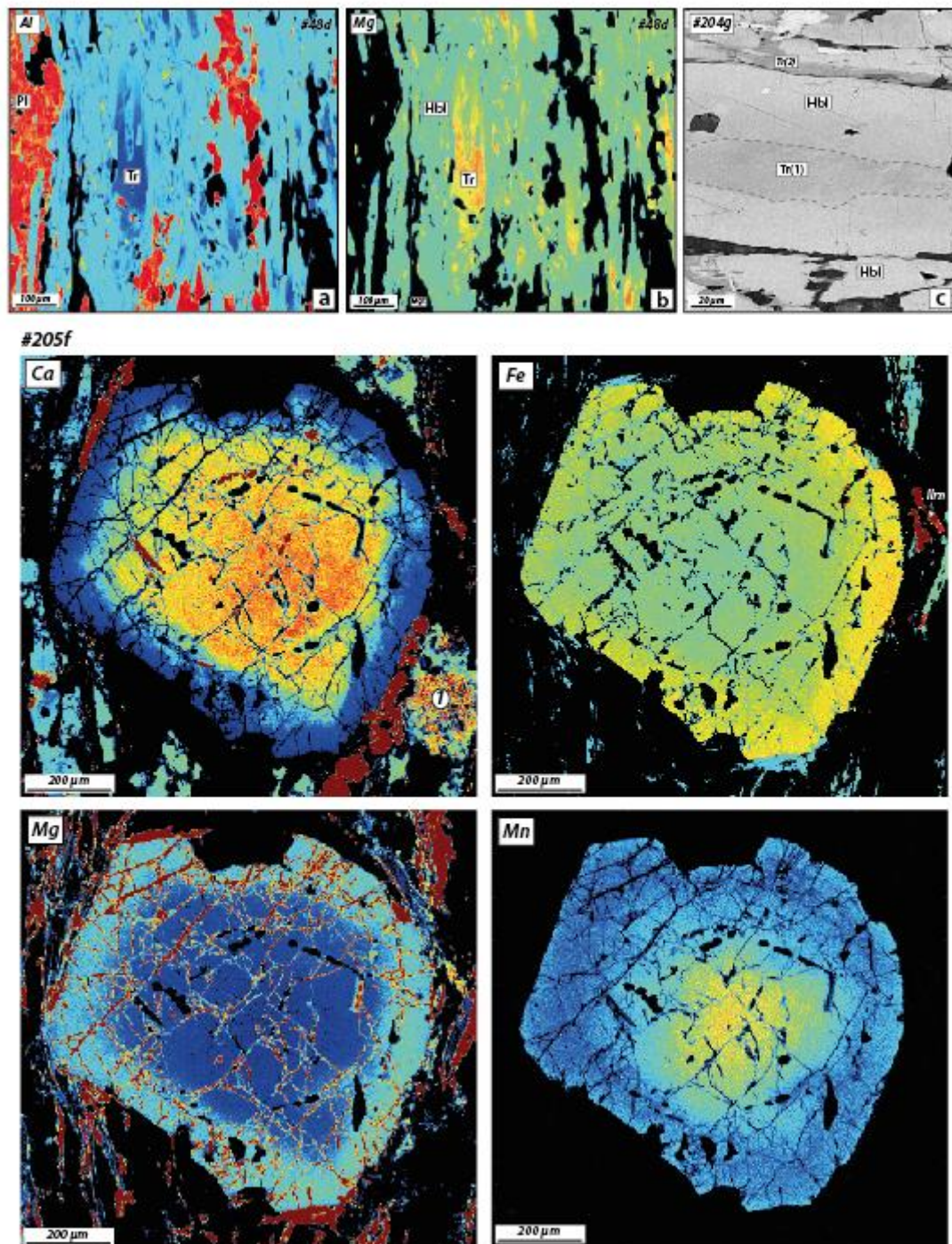


Fig.S2.a,b : X-ray map of an amphibole aggregate in a mafic tuff from the SASZ with tremolitic cores and hornblende-rich rims. c. SEM BSE image showing three generations of amphibole, with tremolitic cores and rims with a hornblende-rich mantle. d. X-ray map of a garnet from a micaschist from the SASZ showing Ca and Mn-richer cores and Fe-Mg richer rims.

Biotite is observed around garnet. Most of the chlorite flakes observed along the foliation are clearly replacing peak biotite. However, in the less deformed facies, biotite has been observed rimming muscovite and also chlorite. Tourmaline is occasionally observed, frequently associated with organic-matter rich layers (**Fig.S1c**). Ilmenite is the main Ti-bearing phase in our samples. It is frequently associated with rutile, which are both rimmed by titanite (**Fig.S1g**). Kyanite has not been found in our samples.

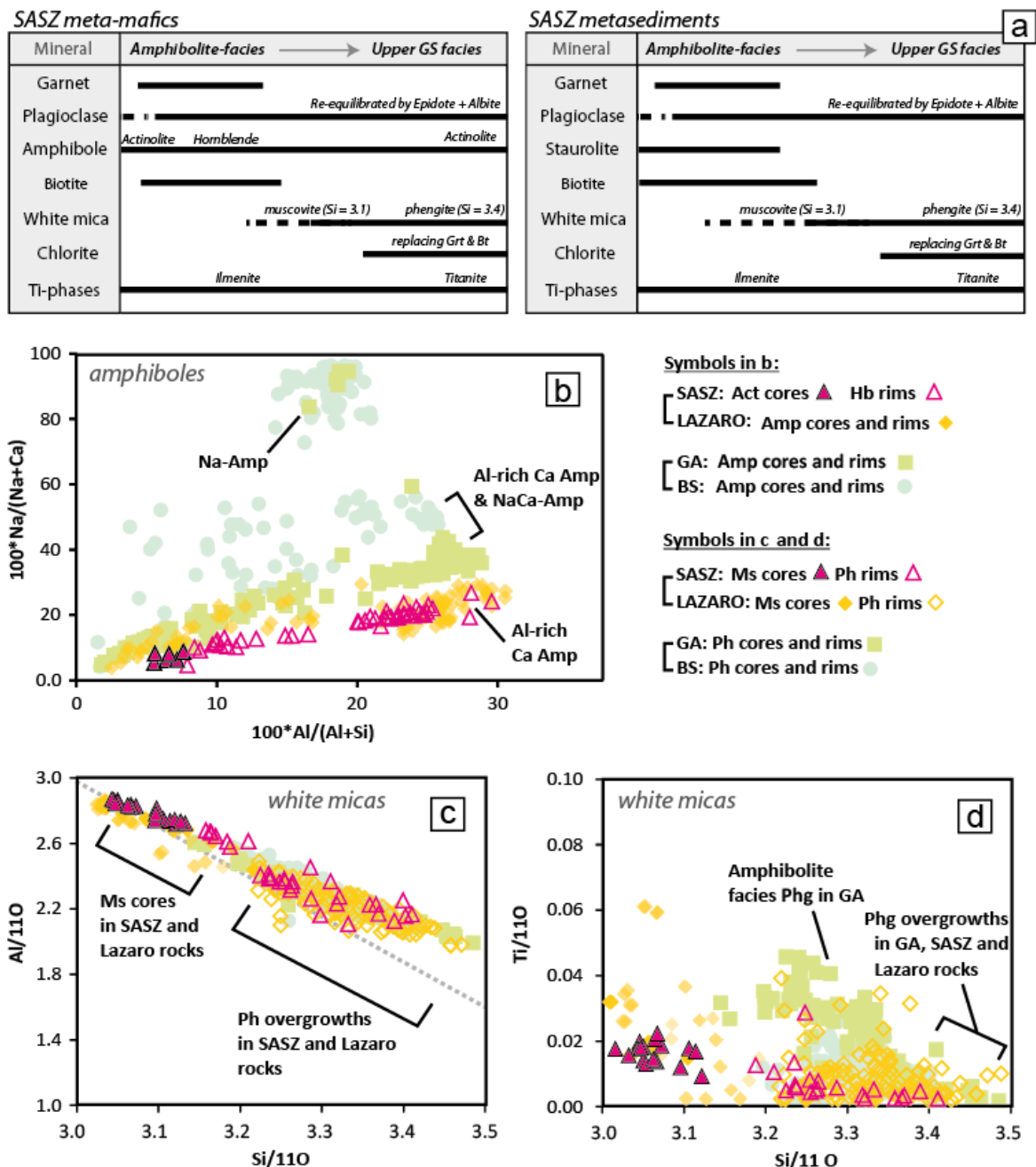


Fig.S3: a. summary of the observed parageneses for SASZ mylonites mafic and sedimentary lithologies. b. Composition of amphibole crystals from the SASZ and comparison with adjacent units. Note how Lazaro and SASZ amphiboles exhibit similar compositions in this diagram. This figure

illustrates that higher pressure amphiboles are found in GA and BS units. c and d. Composition from white micas from SASZ and comparison with adjacent units. Note how similar the phengite overgrowths in SASZ are compared to Lazaro and GA units late phengite rims.

Pseudosection modeling

The P-T location of the peak metamorphic assemblage during the mylonitization stage along the SASZ has been investigated using the pseudosection modeling approach and the software package Perplex (v.6.7.4; Connolly, 2005). In order to obtain the most accurate bulk composition estimate of the mylonitic domain on which we decided to work, we preferred to use an average of five 2 mm² surface composition estimates performed at the scanning electron microprobe (SEM; see Angiboust & Agard, 2010 for details on the method). The sample #48a corresponds to a metapelite comprising garnet, staurolite, biotite, muscovite and chlorite (**Fig.S1d**). The thermodynamic modeling has been performed in the TiNCKFMASH system (manganese and ferric iron, not detected by the EDS detectors at the SEM, have been neglected for simplicity). The estimated bulk composition (in wt.%) used for this calculation is the following: SiO₂(67.92) TiO₂(0.70) Al₂O₃(16.10) FeO(5.04) MgO(1.74) CaO(1.28) Na₂O(2.13) K₂O(2.99). Pure water has been considered in excess for this run. Activity models used here are the following: garnet, staurolite and phengite (Holland & Powell, 1998), biotite (Tajcmanova et al., 2009), orthopyroxene (Powell and Holland, 1999), amphibole (Dale et al., 2005), chlorite (Holland et al., 1998), melt (White et al., 2001 and White et al., 2007), and feldspar (Fuhrman and Lindsley, 1988). The grid has been calculated between 550°C and 700°C and for a pressure range between 0.6 and 1.0 GPa.

The results of this modeling, shown in **figure S4**, enable the identification of a relatively narrow P-T field for which garnet, staurolite, plagioclase, biotite and muscovite are co-stable. This field plots in the pressure range 0.8-0.9 GPa and in the temperature range 600-640°C. Importantly, the presence of garnet in our rock for this composition constrains the minimum pressure and the absence of melt limits the temperature to c.660°C maximum. We used the garnet grossular content isopleths to check the agreement with natural data: measured garnet core grossular contents are between 0.08 and 0.11, which is agreement with modeled garnet composition in

figure S4 (c. 0.10 for the Grt-St field). Similarly, the measured pyrope content is of 0.12 mol.% Prp while the modeled content is 0.13. The Si content of measured muscovite crystal cores is between 3.02 and 3.15 in agreement with modeled Si contents of c.3.11 pfu for the best-fit peak metamorphic conditions. Note that the

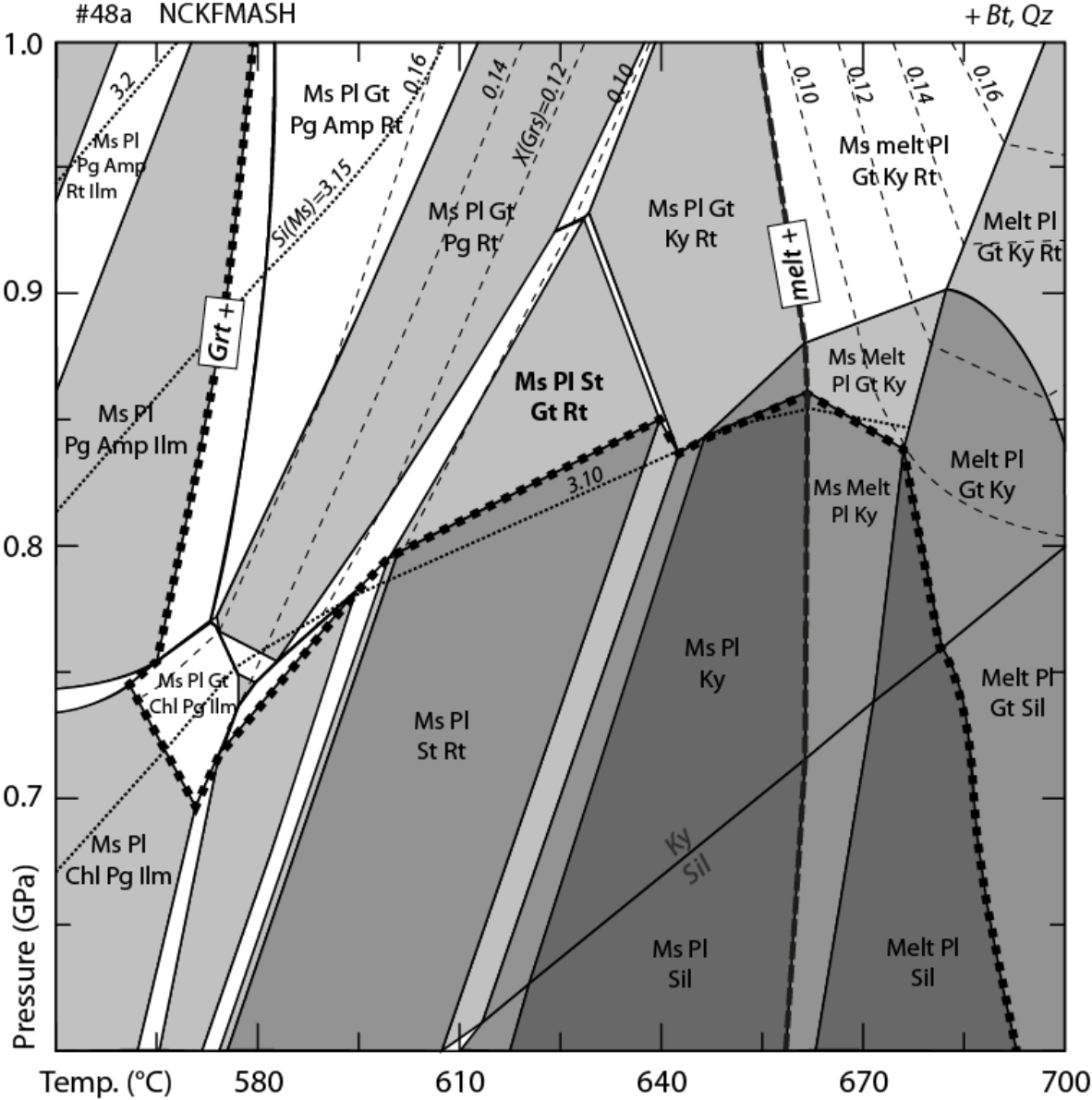


Fig.S4: P-T pseudosection modeling result showing the topology for sample #48a. The best-fit conditions are marked in bold by the assemblage Ms-Pl-St-Gt-Rt-Bt-Qz.

presence of static phengite overgrowths around muscovite with higher Si content (up to 3.32 pfu) implies a decrease in the P/T gradient after mylonitization. Under peak conditions (P=0.86 GPa and T=620°C), the predicted anorthite content of plagioclase is 0.25 which overlaps with the range measured for plagioclase cores (An=0.24-0.3).

Last, the mineral proportions predicted by the modeling at peak conditions are (in vol.%): Grt(2) St(3) Ms(12) Bt(15) Pl(25) Rt(0.2) Qz(43). These proportions are in good agreement with surface estimate proportions performed using optical microscopy (vol.%: Grt(2) St(1) Ms(20) Bt(6) Pl(20) Ilm(0.5) Qz(50)). The only discrepancy between the model and petrological observations concerns the nature of Ti-bearing phases at peak conditions. While the model predicts rutile as the stable phase, the presence of ilmenite inclusions in garnet rather suggests that ilmenite was stable under peak conditions. Given the low amount of TiO₂ in the system, we believe that this slight discrepancy does not significantly affect first-order phase relationships in the model.

References cited

Angiboust, S., & Agard, P. (2010). Initial water budget: The key to detaching large volumes of eclogitized oceanic crust along the subduction channel?. *Lithos*, 120(3), 453-474.

Connolly, J. A. (2005). Computation of phase equilibria by linear programming: a tool for geodynamic modeling and its application to subduction zone decarbonation. *Earth and Planetary Science Letters*, 236(1), 524-541.

Dale, J., Powell, R., White, R. W., Elmer, F. L., & Holland, T. J. B. (2005). A thermodynamic model for Ca–Na clinoamphiboles in Na₂O–CaO–FeO–MgO–Al₂O₃–SiO₂–H₂O–O for petrological calculations. *Journal of Metamorphic Geology*, 23(8), 771-791.

Fuhrman, M. L., & Lindsley, D. H. (1988). Ternary-feldspar modeling and thermometry. *American Mineralogist*, 73(3-4), 201-215.

Holland, T. J. B., & Powell, R. (1998). An internally consistent thermodynamic data set for phases of petrological interest. *Journal of metamorphic Geology*, 16(3), 309-343.

Holland, T., Baker, J., & Powell, R. (1998). Mixing properties and activity-composition relationships of chlorites in the system MgO–FeO–Al₂O₃–SiO₂–H₂O. *European Journal of Mineralogy*, 395-406.

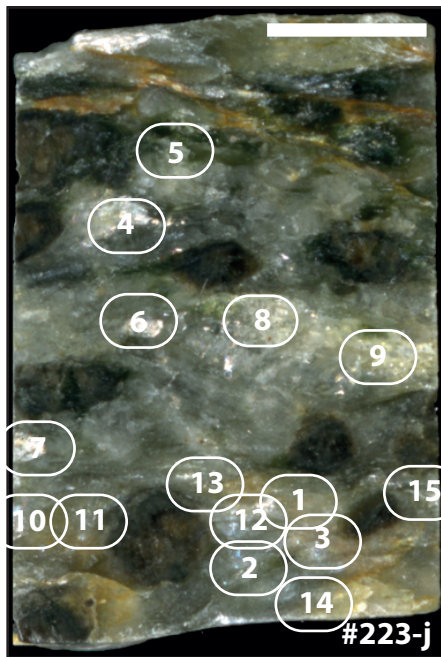
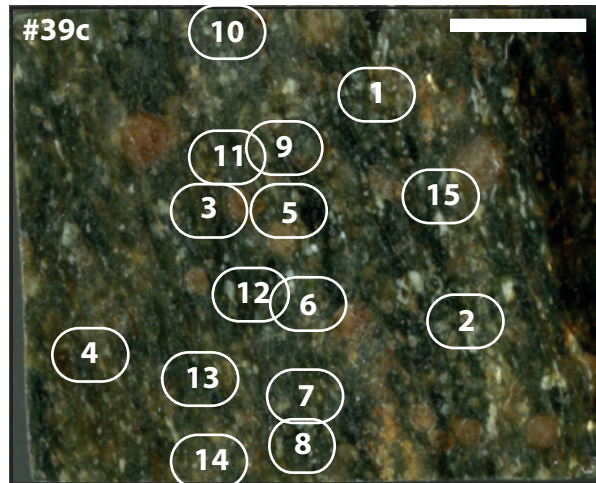
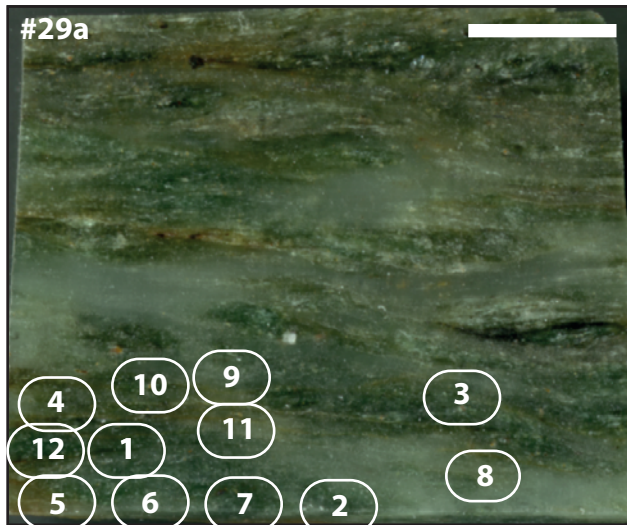
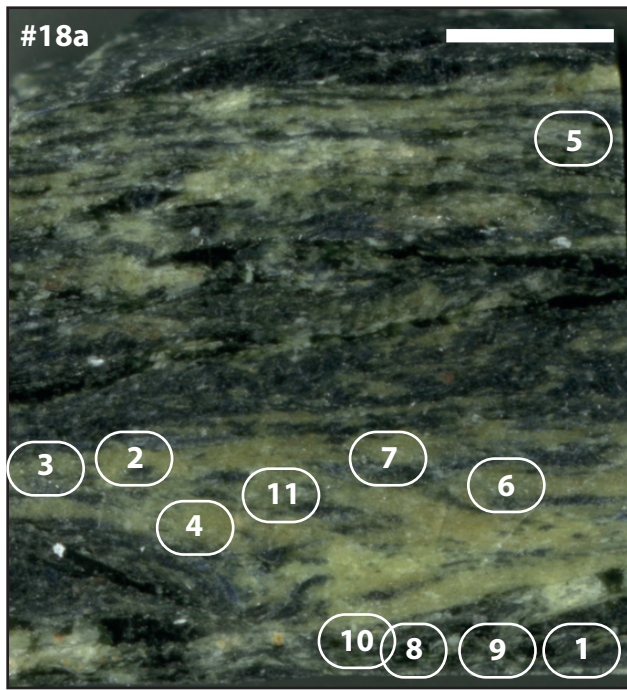
Leake, B. E., Woolley, A. R., Arps, C. E., Birch, W. D., Gilbert, M. C., Grice, J. D., ... & Linthout, K. (1997). Report. Nomenclature of Amphiboles: Report of the Subcommittee on Amphiboles of the International Mineralogical Association Commission on New Minerals and Mineral Names. *Mineralogical magazine*, 61(2), 295-321.

Powell, R., & Holland, T. (1999). Relating formulations of the thermodynamics of mineral solid solutions: activity modeling of pyroxenes, amphiboles, and micas. *American Mineralogist*, 84(1-2), 1-14.

Tajčmanová, L., Connolly, J. A. D., & Cesare, B. (2009). A thermodynamic model for titanium and ferric iron solution in biotite. *Journal of Metamorphic Geology*, 27(2), 153-165.

White, R. W., Powell, R., & Holland, T. J. B. (2007). Progress relating to calculation of partial melting equilibria for metapelites. *Journal of Metamorphic Geology*, 25(5), 511-527.

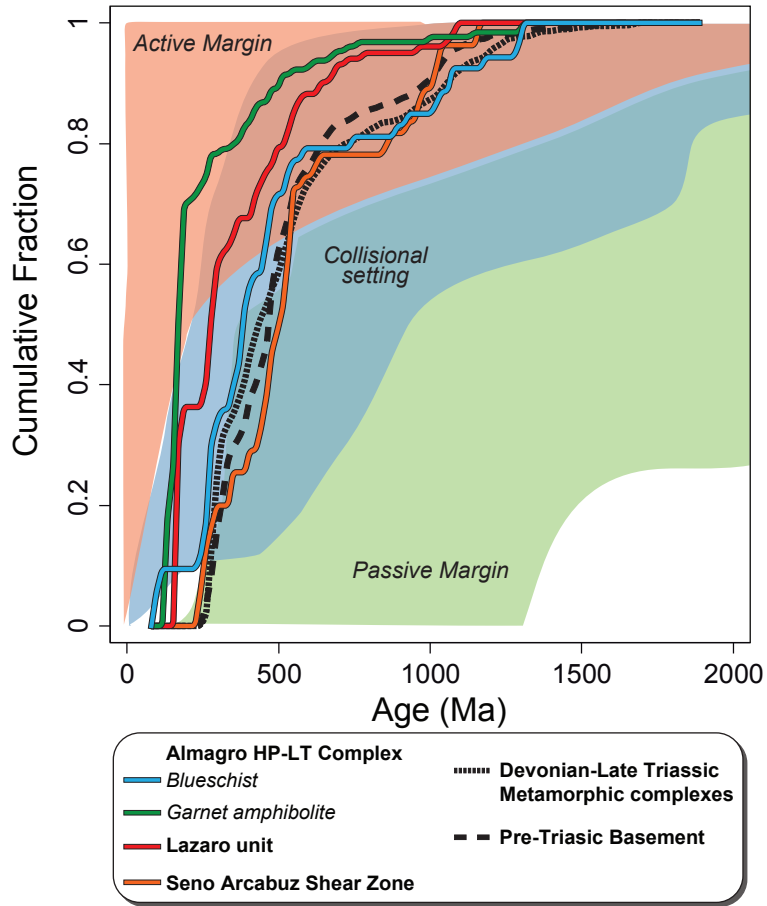
Whitney, D. L., & Evans, B. W. (2010). Abbreviations for names of rock-forming minerals. *American mineralogist*, 95(1), 185.



Electronic appendix 2:

Spot location of *in situ* Ar-Ar analyses.

(white scale bar represents 2.5 mm)



Cawood cumulative probability plots

TABLE DR1. Rb Sr 48b

Sample no. Analysis no.	Material	Rb (ppm)	Sr (ppm)	$^{87}\text{Rb}/^{86}\text{Sr}$	$^{87}\text{Sr}/^{86}\text{Sr}$	$^{87}\text{Sr}/^{86}\text{Sr} \pm 2s_m$
#48b (117.1 ± 2.6 Ma, MSWD = 219, $Sr_i = 0.70518 \pm 0.00063$)						
PS2625	biotite conc. >125 μm	155	14.9	30.3	0.755032	0.0046
PS2626	plagioclase	1.45	6.07	0.69	0.706589	0.0056
PS2722	amphibole	24.0	32.3	2.15	0.708799	0.0021
PS2723	epidote	2.41	151	0.0463	0.704810	0.0029
PS2724	biotite 125-90 μm	199	9.14	63.5	0.808800	0.0022

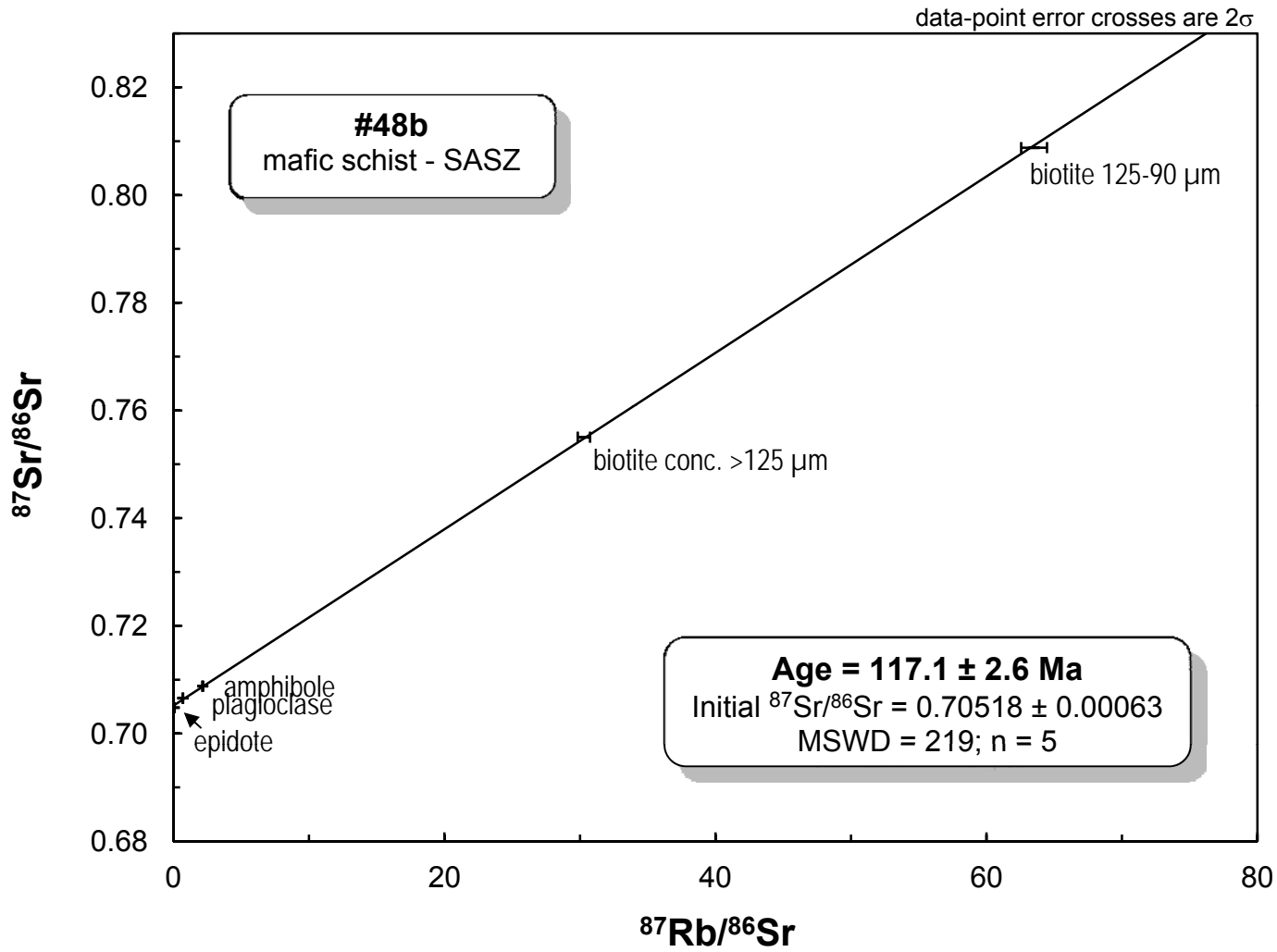


TABLE DR2. Ar-Ar

#24 (Lazaro unit metasediment)

	³⁶ Ar	³⁷ Ar	³⁸ Ar	³⁹ Ar	⁴⁰ Ar	Age ± 2σ (Ma)	⁴⁰ Ar(r) (%)	K/Ca	± 2σ	
#1	0.0873466	0.0356136	0.0012677	15.06000	287.1194	127.80	± 0.73	91.71	181.8	± 8412.4
#2	0.0999976	1.4797592	0.0200299	9.73323	163.8182	113.29	± 0.84	84.68	2.8	± 3.0
#3	0.0413473	0.0000000	0.0046705	16.15813	312.2876	129.50	± 0.66	96.19	0.0	± 0.0
#4	0.0801325	1.0284619	0.0000000	14.34546	255.9892	119.89	± 0.66	91.49	6.0	± 8.0
#5	0.0754119	4.7795608	0.0515167	8.74795	126.4341	97.70	± 0.81	84.97	0.8	± 0.4
#6	0.0381377	0.2017407	0.0511773	13.70673	200.8439	99.02	± 0.61	94.63	29.2	± 192.3
#7	0.0625773	0.4707187	0.0613541	14.50499	266.0736	123.13	± 0.64	93.46	13.3	± 34.0
#8	0.0396315	0.0000000	0.0533768	10.38763	182.4139	118.04	± 0.84	93.92	0.0	± 0.0
#9	0.9579532	4.5819592	0.0132815	13.34143	247.6784	124.56	± 2.12	46.65	1.3	± 0.5
#10	0.0190125	0.0000000	0.0000000	14.31742	280.7659	131.33	± 0.55	97.99	0.0	± 0.0
#11	0.0977346	0.0000000	0.0344353	14.61806	227.5515	105.02	± 0.51	88.69	0.0	± 0.0
#12	0.2926610	0.0000000	0.0000000	13.43855	259.0958	129.19	± 0.89	74.95	0.0	± 0.0
#13	0.1271525	0.0000000	0.0643839	4.37491	63.8573	98.65	± 1.48	62.93	0.0	± 0.0
#14	0.0670986	0.0000000	0.0526429	5.72754	86.1264	101.55	± 0.86	81.24	0.0	± 0.0
					<i>Average</i>	115.62	± 0.87			
					<i>Std dev.</i>	12.81				
					2 populations of white mica	<i>average 1</i>	124.08	muscovite		
						<i>Std dev.</i>	6.06			
						<i>average 2</i>	100.39	phengite		
						<i>Std dev.</i>	2.95			

TABLE DR2. Ar-Ar

#29a (Lazaro unit basal phyllonite)

	³⁶ Ar	³⁷ Ar	³⁸ Ar	³⁹ Ar	⁴⁰ Ar	Age ± 2σ (Ma)	⁴⁰ Ar(r) (%)	K/Ca	± 2σ	
#1	0.0178687	1.599615	0.0170733	2.312508	26.60458	78.20	± 2.14	83.38	0.622	± 1.118
#2	0.0280345	2.087189	0.0000000	1.929777	22.15203	78.03	± 2.52	72.74	0.398	± 0.462
#3	0.0242715	1.937818	0.0000000	1.395878	15.94420	77.65	± 3.15	68.93	0.310	± 0.366
#4	0.0164722	1.212813	0.0000000	1.569039	16.84632	73.08	± 2.61	77.53	0.556	± 0.843
#5	0.0281132	2.048319	0.0284595	3.139143	32.71550	70.98	± 1.48	79.69	0.659	± 0.649
#6	0.0201950	0.996153	0.0256693	3.136126	32.73983	71.10	± 1.45	84.52	1.354	± 3.763
#7	0.0159289	4.244555	0.0132117	5.399020	59.72117	75.25	± 0.92	92.62	0.547	± 0.239
#8	0.0334196	1.796761	0.0212667	0.969188	12.14753	85.03	± 4.68	55.13	0.232	± 0.277
#9	0.0402772	3.590630	0.0644562	3.776369	38.38533	69.26	± 1.22	76.28	0.452	± 0.259
#10	0.0400912	1.964154	0.0196967	3.551521	37.52774	71.95	± 1.34	75.95	0.778	± 0.860
#11	0.0193740	2.172920	0.0643819	2.957517	29.93288	68.97	± 1.35	83.88	0.585	± 0.594
#12	0.0162087	2.662421	0.0318260	2.507185	26.21434	71.21	± 1.79	84.49	0.405	± 0.386
					<i>Average</i>	73.24	± 1.82			
					<i>Std dev.</i>	3.47				

TABLE DR2. Ar-Ar

#39a (micaschist, Garnet amphibolite unit)

	³⁶ Ar	³⁷ Ar	³⁸ Ar	³⁹ Ar	⁴⁰ Ar	Age ± 2σ (Ma)	⁴⁰ Ar(r) (%)	K/Ca	± 2σ
#1	0.0187041	7.519825	0.0340463	3.653741	53.76238	99.42 ± 1.69	90.62	0.209	± 0.053
#2	0.0327158	1.085463	0.0296989	1.893989	32.53380	115.54 ± 3.94	77.06	0.750	± 1.072
#3	0.0419768	3.345609	0.0370542	2.250929	36.92024	110.49 ± 2.80	74.82	0.289	± 0.141
#4	0.0526503	9.135966	0.0420852	4.853729	73.53957	102.29 ± 1.39	82.49	0.228	± 0.034
#5	0.0408121	5.907393	0.0193404	3.280736	50.90700	104.69 ± 2.15	80.81	0.239	± 0.068
#6	0.0464245	2.888551	0.0759786	3.994957	59.23844	100.17 ± 1.74	81.15	0.595	± 0.281
#7	0.0397181	2.891458	0.0500858	3.252089	50.91986	105.61 ± 2.02	81.23	0.484	± 0.238
#8	0.0578002	2.051999	0.0548254	2.253539	41.49743	123.59 ± 4.05	70.82	0.472	± 0.568
#9	0.0708177	3.226092	0.0423047	1.799768	29.11814	109.03 ± 3.69	58.16	0.240	± 0.113
#10	0.0777029	2.646496	0.0811749	2.505496	41.39514	111.27 ± 2.83	64.30	0.407	± 0.223
#11	0.0310758	3.276818	0.0190090	4.323943	60.63759	94.88 ± 1.38	86.80	0.567	± 0.315
#12	0.0528357	2.340278	0.0383986	4.397778	65.57382	100.71 ± 1.49	80.73	0.808	± 0.526
#13	0.0887393	1.237711	0.0670744	1.565568	27.51280	118.13 ± 5.09	51.19	0.544	± 1.158
#14	0.0607358	1.501590	0.0505198	2.962345	42.64945	97.34 ± 2.36	70.35	0.848	± 1.284
				<i>Average</i>	106.65	± 2.62			
				<i>Std dev.</i>	8.40				
				<i>Average age corrected</i>	102.69	1.99			
				<i>Std dev.</i>	5.35				

TABLE DR2. Ar-Ar

#223J (westernmost exposure of blueschist unit micaschists)

	³⁶ Ar	³⁷ Ar	³⁸ Ar	³⁹ Ar	⁴⁰ Ar	Age ± 2σ (Ma)	⁴⁰ Ar(r) (%)	K/Ca	± 2σ
#1	0.0215075	1.574922	0.0730032	8.87393	81.1084	62.40 ± 0.52	92.64	2.42	± 3.60
#2	0.0197058	0.000000	0.0044423	12.67907	117.3169	63.16 ± 0.41	95.18	0.00	± 0.00
#3	0.0219912	1.783771	0.0021983	11.00414	97.8300	60.72 ± 0.43	93.68	2.65	± 3.37
#4	0.0177940	0.962936	0.0245452	12.48805	127.4591	69.54 ± 0.43	95.95	5.58	± 14.50
#5	0.0352716	0.362482	0.0000000	11.23834	117.0737	70.95 ± 0.48	91.75	13.33	± 82.58
#6	0.0137325	0.334653	0.0000000	11.87851	122.4805	70.24 ± 0.47	96.71	15.26	± 99.07
#7	0.0201583	0.000000	0.0053757	11.66609	110.9723	64.90 ± 0.44	94.81	0.00	± 0.00
#8	0.0255382	0.000000	0.0484298	10.82801	109.9603	69.20 ± 0.48	93.49	0.00	± 0.00
#9	0.0203947	1.158349	0.0000000	13.57298	138.6268	69.59 ± 0.41	95.75	5.04	± 10.43
#10	0.0324134	0.438560	0.0000000	6.86268	70.4025	69.89 ± 0.72	87.95	6.73	± 34.76
#11	0.0117157	1.708011	0.0000000	13.28933	133.0983	68.26 ± 0.41	97.37	3.35	± 4.93
#12	0.0180306	1.180104	0.0000000	13.46155	131.0419	66.38 ± 0.43	96.00	4.91	± 6.52
#13	0.0224635	2.924965	0.0000000	7.83478	67.9823	59.29 ± 0.67	91.01	1.15	± 0.59
#14	0.0638670	0.220869	0.0025568	11.04717	112.9269	69.65 ± 0.54	85.61	21.51	± 134.96
					<i>Average</i>	66.73			
					<i>Std dev.</i>	3.92			

TABLE DR2. Ar-Ar

#18a (blueschist unit metatuff)

	³⁶ Ar	³⁷ Ar	³⁸ Ar	³⁹ Ar	⁴⁰ Ar	Age ± 2σ (Ma)	⁴⁰ Ar(r) (%)	K/Ca	± 2σ
#1	0.0148100	1.452048	0.0434041	10.577338	119.36386	76.73 ± 0.54	96.38	3.132	± 3.117
#2	0.0073616	7.956414	0.0446726	6.551277	76.69534	79.54 ± 0.78	97.16	0.354	± 0.053
#3	0.0119078	13.319770	0.0203247	6.376068	73.01742	77.85 ± 0.83	95.33	0.206	± 0.022
#4	0.0182873	11.683316	0.0000000	5.613803	68.11390	82.37 ± 1.03	92.58	0.207	± 0.024
#5	0.0198125	9.258329	0.0160989	6.873476	78.95218	78.08 ± 0.84	93.02	0.319	± 0.100
#6	0.0170591	12.174758	0.0123050	5.365132	63.40768	80.28 ± 1.00	92.57	0.189	± 0.023
#7	0.0432480	8.186590	0.0128231	4.594551	56.94599	84.11 ± 1.27	81.62	0.241	± 0.034
#8	0.0167046	0.390570	0.0000000	15.692934	177.02689	76.71 ± 0.40	97.21	17.277	± 101.167
#9	0.0346193	10.132693	0.0276943	3.886250	45.93047	80.29 ± 1.45	81.73	0.165	± 0.020
#10	0.0168088	10.241151	0.0087877	4.859607	57.15077	79.90 ± 1.06	91.93	0.204	± 0.037
					<i>Average</i>	79.59			
					<i>Std dev.</i>	2.38			

TABLE DR4. GPS coordinates

Sampling locality	Latitude (S)	Longitude (W)
# 18	51° 36' 12"	75° 12' 06"
# 24	51° 32' 24"	75° 09' 19"
# 29	51° 35' 13"	75° 11' 14"
# 39	51° 34' 26"	75° 12' 35"
# 43	51° 37' 22"	75° 12' 23"
# 47	51° 34' 52"	75° 11' 59"
# 48	51° 27' 33"	75° 08' 43"
#223	51° 38' 04"	75° 18' 19"

GPS Coordinates of studied sampling localities